LABORATORY TESTING AND NUMERICAL MODELLING OF THE DYNAMIC BEHAVIOUR OF TAGUS RIVER SAND

Luís Miranda*, *MSc, Laboratório Nacional de Engenharia Civil, lmiranda@lnec.pt*

Laura Caldeira, *PhD, Laboratório Nacional de Engenharia Civil, laurac@lnec.pt*

João Serra, *PhD, Laboratório Nacional de Engenharia Civil, biles@lnec.pt*

André Barbosa, *PhD, Oregon State University, andre.barbosa@oregonstate.edu*

ABSTRACT

In the framework of a third Tagus River crossing, through an immersed tunnel, advanced laboratory tests were performed on its highly liquefiable foundation sand, namely cyclic undrained torsional tests. The Manzari-Dafalias model, which allows simulating liquefaction on the Tagus River sand and is, therefore, central in the tunnel design, as well as the numerical work to calibrate the model and identify its most relevant parameters, are presented. Model parameters, their respective reference values and tests performed to determine directly most of the parameters, are introduced. A parameter sensitivity analysis, conducted through numerical simulation of triaxial monotonic drained tests and of cyclic undrained torsional tests, implemented both for the pre-liquefaction and liquefaction phases, is described. Finally, some parameters are determined by fitting the model to the laboratory results.

Keywords: advanced laboratory tests, constitutive model, numerical simulation, liquefaction, immersed tunnel.

1. INTRODUCTION

Design of a third Tagus river crossing is currently being considered downstream of 25 de Abril Bridge in Lisbon, Portugal, between Algés and Trafaria, corresponding to an immersed tunnel with a length of approximately 2.4 km.

Many immersed tunnels are built on alluvial formations in earthquake zones and one of the main issues in their safety design is precisely their resistance to foundation liquefaction. As a matter of fact, displacements of an immersed tunnel resulting from a seismic event depend largely on the behaviour of the surrounding ground, namely its stiffness [1]. These displacements may be amplified by liquefaction and can lead to ground failure if significant loss of soil strength occurs. Consequences of liquefaction may include loss of lateral or vertical support, differential movements or rotations, movements due to shake-down settlement effects (where granular material naturally densifies due to loss of structure) and floatation of the tunnel. Likewise, its uncontrolled movement is undesirable and could lead to overstressing and damage of the structure or leakage of the tunnel joints.

This paper summarizes the laboratory and numerical work to calibrate a chosen constitutive model, the Manzari-Dafalias (M-D) model, to the Tagus river sand properties, with the goal of enabling its future application in the scope of the immersed tunnel crossing design.

2. TAGUS RIVER SAND

The immersed tunnel is supported on alluvial Tagus river sands, with a maximum thickness of around 50 m, overlaying Miocenic layers of increasing stiffness and strength with depth and a basalt bedrock (Figure 1). The river maximum depth is about 30 m.

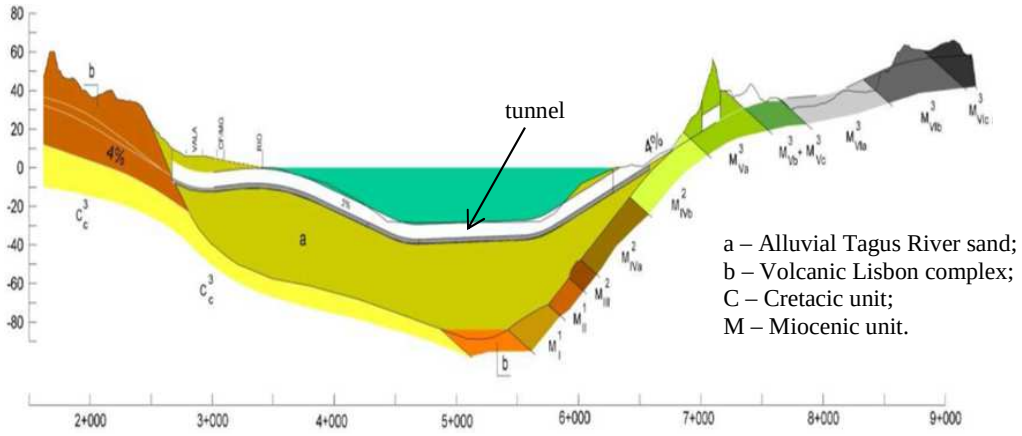

Figure 1. *Third Tagus River crossing geologic profile*

Tagus River sand is a siliceous, clean and poorly graded sand, classified as SP. Its physical characterization included: a grain size analysis; determining the solid particles density, G_S; and obtaining the maximum, $\gamma_{d,max}$, and minimum, $\gamma_{d,min}$, dry unit weight. Some physical indexes are presented in Table 1.

Table 1. *Physical indexes of Tagus River sand*

D_{10}	0.20 mm	D_{50}	0.36 mm	$\gamma_{d,max}$	17.12 kN/m^3
D_{30}	0.28 mm	G_S	2.70	$\gamma_{d,min}$	14.32 kN/m^3

The in-situ relative density, D_r, of Tagus River sand was determined by using a correlation with SPT values, which were obtained for different boreholes and depths, mainly in the north shore of the river. Similar SPT values were assumed at the centre of the river as, at the tunnel site, flow velocities near the bed of the waterway are small. A D_r of 70% was then obtained. Admitting a maximum depth of 30 m for liquefaction triggering, effective confining pressures, p_{conf}, ranging from 100 to 300 kPa, were set. Additionally, $D_r = 60\%$ ($p_{conf} = 100\ kPa$) and $D_r = 80\%$ ($p_{conf} = 300\ kPa$) were adopted to analyse the effect of varying the relative density. All stresses herein defined are effective stresses.

3. CYCLIC UNDRAINED TORSIONAL TESTING

Actuation of the earthquake generates primarily an increase of shear stresses, which can be well simulated in a cyclic torsional test. Thus, the main goal of these tests was to characterize stress-strain behaviour of the sand under cyclic loading, in the medium to large range of strains, including liquefaction, and to obtain parameters for the constitutive model, related with dynamic behaviour of the soil.

Therefore, LNEC's (Laboratório Nacional de Engenharia Civil) torsional shear device [2] was used to perform five cyclic undrained torsional tests (CUTTs) on hollow cylindrical specimens. Table 2 includes dimensions of the specimens, H_0, $r_{e,0}$ and $r_{i,0}$, as well as their dry unit weight, γ_d, relative density, D_r, and void ratio after preparation, e_0; the chosen effective consolidation pressure, p_{conf}, and void ratio after consolidation phase, e_{conf}.

Table 2. *Cyclic undrained torsional tests data*

	After specimen preparation						After consolidation	
Test	H_0 (m)	$r_{e,0}$ (m)	$r_{i,0}$ (m)	γ_d (kN/m^3)	D_r (%)	e_0	p_{conf} (kPa)	e_{conf}
CUT_Dr70_p300	0.1431	0.0354	0.0147	16.15	68.9	0.640	300	0.551
CUT_Dr70_p200	0.1433	0.0354	0.0148	16.17	69.8	0.637	200	0.581
CUT_Dr70_p100	0.1431	0.0355	0.0147	16.18	70.0	0.637	100	0.627
CUT_Dr60_p100	0.1431	0.0355	0.0147	15.92	60.9	0.664	100	0.652
CUT_Dr80_p300	0.1433	0.0355	0.0147	16.51	80.6	0.605	300	0.539

After the saturation phase, specimens were isotropically consolidated. All tests were subjected to shear by controlling strain. Strain amplitude, $\gamma_{\theta z}$, was increased progressively seven times, using each of the following values during 10 cycles of 1 s ($f = 1$ Hz): $\gamma_{\theta z} = \pm 5\times10^{-4}, \pm 1\times10^{-3}, \pm 3\times10^{-3}, \pm 6\times10^{-3}, \pm 1.0\times10^{-2}, \pm 2.0\times10^{-2}, \pm 3.0\times10^{-2}$.

External and internal confining pressures were kept constant as well as axial force. Changes on the mean effective confining stress were exclusively due to pore pressure variation. Additionally, the final excess pore pressure value corresponded approximately to the initial mean effective confining stress, which meant liquefaction was attained in all cases.

Figure 2 to Figure 4 illustrate the obtained results for test CUT_Dr70_p100, with a D_r of 70% and the lowest p_{conf} of 100 kPa. Initial liquefaction was considered to have occurred when excess pore pressure was 95% of the initial effective consolidation pressure, thus in this test at cycle 47 ($\gamma_{\theta z} = \pm 0.01$ - Figure 4).

In Figure 2, it can be observed that, for the first cycles, the curves are very close together, but as the specimen approaches liquefaction strains increase and hysteresis loops' open up quickly, tending to the horizontal, with their hysteresis area increasing considerably.

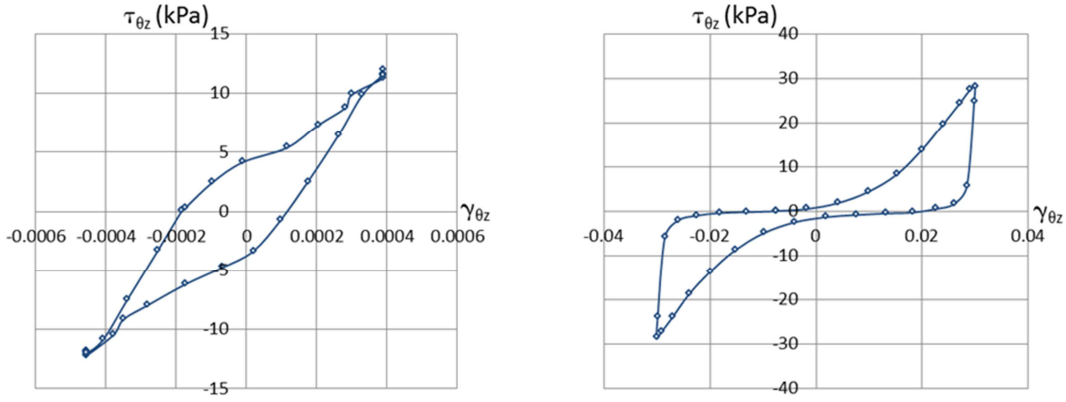

Figure 2. *Shear stress $\tau_{\theta z}$ (kPa) vs shear strain $\gamma_{\theta z}$ (left - cycle 6 (pre-liquefaction); right - cycle 66 (liquefaction))*

Concerning Figure 3, the left plot reflects the gradual build-up of pore pressure (Figure 4) as the effective mean stress reduces. Before initial liquefaction, for each imposed strain, the decrease in p, as well as the rate of excess pore water pressure accumulation, is higher during the first cycle than during the subsequent cycles, where it is almost constant. This behaviour has been associated with particle rearrangement and elimination of local instabilities at the contact points [3].

The specimen starts failing, as the stress path approaches the critical stress ratio. As seen on the right plot of Figure 3, the shape of the stress path changes completely and becomes "hooked" towards the later stages of the test. The specimen reaches the critical stress ratio at

low q values, because of the high pore pressures generated, but as strain increases dilation tendency moves the stress path up the critical state line (CSL). When stress reverses, dilation tendency ceases and volumetric contraction tendency drives the stress path back down towards the origin, until the critical stress ratio is encountered in the opposite direction. Moreover, for each cycle of imposed shear strain, there are two cycles of excess pore pressure, which decreases in the dilation phase and, after strain (and stress) reversal, increases in the contraction phase in both directions.

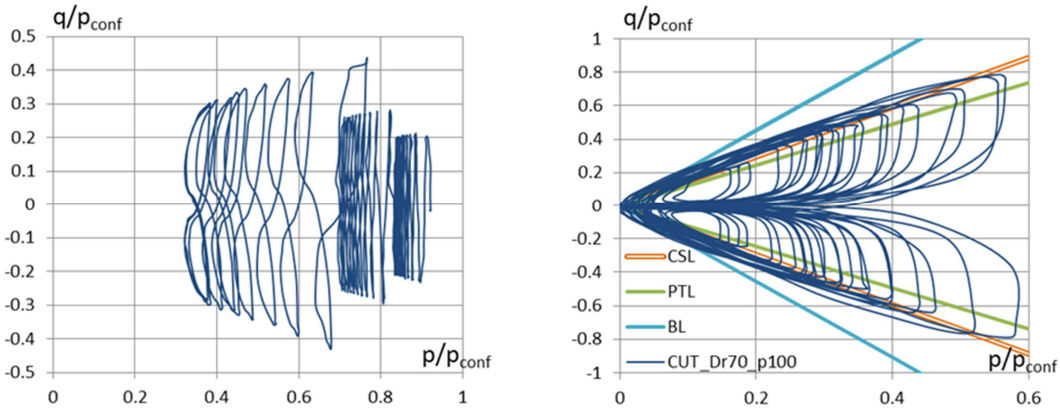

Figure 3. *q/p_{conf} vs p/p_{conf} (left – cycles 1 to 30 (pre-liquefaction); right - after initial liquefaction; CSL – critical state line, PTL – phase transformation line, BL – bounding line)*

After cycle 20, when a shear strain amplitude of ±3x10^{-3} was imposed, sand began to become significantly soft and pp/p_{conf}, at the end of the last cycle with this amplitude (cycle 30), exceeded approximately 65% (Figure 4).

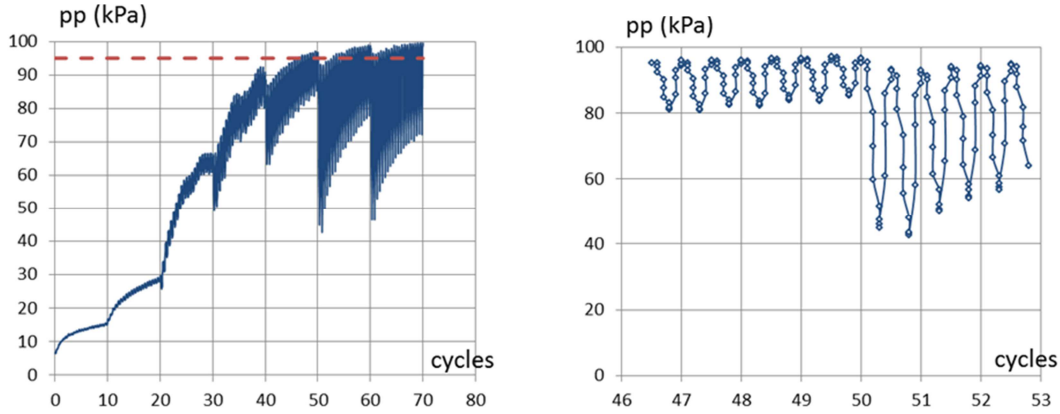

Figure 4. *Excess pore pressure pp (kPa) vs number of cycles (left – full test; right - detail after initial liquefaction)*

4. NUMERICAL MODELLING OF THE LABORATORY TESTS

4.1. Constitutive Model

The Manzari-Dafalias (M-D) model was chosen. This bounding surface model builds upon previous work by [4], which was extended to account for the effect of fabric changes during loading [5]. In the formulation in triaxial stress space, the yield surface represents a ‘‘wedge’’ in *p-q* space, with an opening value of $2mp$ and whose bisecting line has a slope α (Figure 5). α and m are stress ratio quantities. The dilatancy line, where there is a zero volumetric rate response, separates the contractant (below the line) from the dilatant (over the line) response.

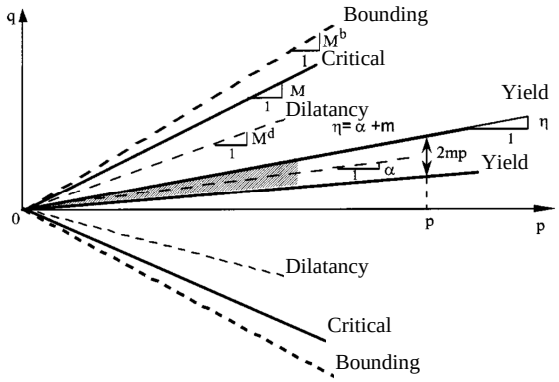

Figure 5. *Yield, critical (CSL), dilatancy (PTL) and bounding lines (BL) in p-q space [5]*

The model parameters and respective reference values, which correspond either to laboratory tests results ([lab]) or to published data in several references about the M-D model ([5], [6], [7], [8]), plus tests commonly used to determine the parameters, are summarized in Table 3.

The following parameters of the M-D model were directly determined from MDTTs: $G_0 = 125$ and $\nu = 0.3$ (elasticity parameters); $M_{f,c} = 1.46$, $c = 0.67$, $e_{p0} = 0.014$, $\lambda_c = 0.78$ and $\xi = 1.15$ (related with the critical state); $n^b = 3.5$ (related with the plastic modulus) and $A_0 = 0.932$ and $n^d = 1.5$ (related with dilatancy).

Table 3. *Manzari-Dafalias model parameters, reference values and published data*

Category	Parameter	Reference value	Test
Physical	γ_d	16.21 kN/m^3 [lab]	Physical testing
	e_0	0.634 [lab]	Physical testing (Dr = 71.3%)
Elasticity	G_0	125 [lab] [8]	RCT (small strain measurements), MDTT
	ν	0.3 [lab] (0.2 to 0.4 in [7])	MDTT, $\nu = \frac{K_0}{1+K_0}$ $K_0 = 1 - sin\phi$
Critical state	$M_{f,c}$	1.46 [lab] (1.20 to 1.32 in [7])	MDTT
	c	0.67 [lab]	MDTT ($c = M_{f,e}/M_{f,c}$)
	λ_c	0.014 [lab] (0.01 to 0.03 in [7])	MDTT that approach critical state
	e_{p0}	0.78 [lab] (0.72 to 0.90 in [7])	Void ratio at $p_c = 1kPa$. MDTT that approach critical state
	ξ	1.15 [lab] (0.7 for most sands [6])	MDTT that approach critical state
Yield surface	m	0.015 [8] (0.02-0.05 in [6] and 0.06-0.07 in [7])	Fitting (MDTT)
Plastic modulus	h_0	7.05 [8]	Fitting (MDTT)
	c_h	0.968 [8]	Fitting (MDTT)
	n^b	3.5 [lab] (1.1 in [5])	$n^b = \ln(\frac{M}{M^b})/\Psi^b$, where Ψ^b and M^b are the values of Ψ and η at a drained peak stress ratio state
Dilatancy	A_0	0.932 [lab] (0.704 in [5])	MDTT – good quality stress dilatancy data – volumetric strain vs deviatoric strain in a constant p drained triaxial test (before z is activated $A_0 = A_d$)
	n^d	1.5 [lab] (3.5 in [5])	$n^d = \ln(\frac{M}{M^d})/\Psi^d$, where Ψ^d and M^d are the values of Ψ and η at a phase transformation state
Fabric-dilatancy tensor	z_{max}	4 [8] (4-5 for most sands in [6])	Fitting (CUTT) – η must exceed M^d so that the evolution of z is activated
	c_z	600 [8]	Fitting (CUTT) - η must exceed M^d so that the evolution of z is activated

MDTT - monotonic drained triaxial test; RCT - resonant column test; CUTT - cyclic undrained torsional test.

4.2. Sensitivity analysis

Before calibrating the remaining parameters, related to monotonic and cyclic behaviour, a sensitivity analysis was carried out in order to better understand the relevance of each model parameter. The selected parameters were namely those that couldn't be obtained directly by laboratory tests (m, h_0 and c_h) as well as some parameters that, though obtained directly through laboratory tests, don't have a straight physical meaning (n^b, A_0 and n^d). G_0 was also considered due to its relevance in the response, particularly in the pre-liquefaction phase.

Numerical simulations of laboratory tests, MDTTs and CUTTs, were performed using an existing OpenSees constitutive driver [8], where the Manzari-Dafalias model governing equations had been implemented. The numerical model was built to perform the described sensitivity analysis, using a 1x1x1 m^3 SSPbrickUP 3D element with 8 nodes. This element can be used in dynamic analysis of saturated porous media with a mixed displacement-pressure ($u-p$) formulation, based upon the work of Biot as extended by [9].

A variation of ±20% of the reference value was defined for the selected parameters (except for parameter m, for which, according to several references, 0.015, 0.03 and 0.06 were chosen). This ±20% variation was believed adequate to avoid instabilities and non-convergence of the model. Only the main results of the sensitivity analysis through numerical simulation of MDTTs are presented next, since it is described in more detail in [10].

4.2.1. Parameter Sensitivity Analysis through Numerical Simulation of MDTTs

Results of the sensitivity analysis for each model parameter pointed out that the parameters that cause a greater variation of the response are: c_h concerning peak shear strain ε_s, n^b regarding peak shear stress ratio η and finally A_0 concerning peak dilatancy and volumetric strain at the critical state ε_V. Then, two related parameters (A_0 with n^d concerning dilatancy and c_h with h_0 regarding the plasticity modulus) were varied simultaneously. It was shown that when parameters c_h and h_0 are varied simultaneously, ε_s variation is fairly greater than when only one of them is changed. Finally, pairs of the most relevant parameters (A_0 with c_h, A_0 with n^b and c_h with n^b), were also varied simultaneously. It was concluded that joint variation of parameters c_h and A_0 causes larger variation than when only one of the parameters is changed.

4.2.2. Parameter Sensitivity Analysis through Numerical Simulation of CUTTs

First, specific boundary conditions for the SSPbrickUP 3D element had to be defined. At the base of the element two of the four nodes were free in each horizontal direction (x or y) and one was free in both horizontal directions. The top nodes were all free. During the consolidation phase, concentrated forces representing an all-around confining pressure p_{conf} (100, 200 or 300 kPa) were applied at the free nodes. Then, in the shear phase, pore pressure was set free at all nodes and top nodes were fixed in the horizontal direction (y). Displacements were applied at the four top nodes in the x horizontal direction, according to a cyclic sine function, with a frequency of 1 Hz and which amplitude increases progressively up to ±0.03 m (±1x10^{-5}, ±5x10^{-5}, ±1x10^{-4}, ±5x10^{-4}, ±0.001, ±0.003, ±0.006, ±0.01, ±0.02 and ±0.03 m).

Parameters c_z and z_{max} weren't considered in the *pre-liquefaction phase* because they only have influence on liquefaction response. From the analysis of 3 cycles gradually approaching liquefaction, it was concluded that the most relevant parameters for cyclic response in this phase are G_0, m, h_0 and c_h. In Figure 6, the normalized stress path q/p_{conf} vs p/p_{conf} for the pre-liquefaction phase and the pore pressure ratio change during the shear phase are shown, considering the effect of changing parameter G_0 in the response.

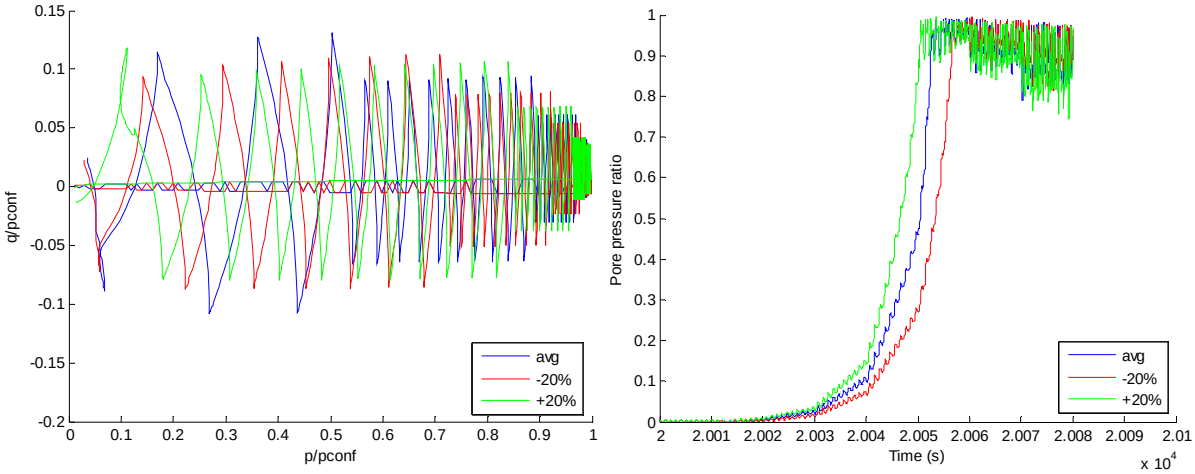

Figure 6. *q/p_{conf} vs p/p_{conf} paths (pre-liquefaction) and pore pressure ratio time history (shear phase) considering variation of G_0*

In Figure 7, the normalized stress path q/p_{conf} vs p/p_{conf} for 3 cycles in the *liquefaction phase* (corresponding to different applied shear strain levels, respectively ±0.01, ±0.02 and ±0.03) is presented, considering the influence of varying c_z in the response. In the liquefaction phase, in each cycle, the pore pressure ratio should reach a value near one and shear strain should follow the applied cyclic displacements. However, due to convergence problems of the M-D model, the pore pressure ratio varies significantly, with its maximum value decreasing and moving away from one and shear strain doesn't follow the applied cyclic displacements (Figure 7). Thus, it wasn't possible to determine the relative importance of c_z and z_{max} in cyclic response. Further improvements in the M-D model are deemed necessary, namely for the liquefaction phase.

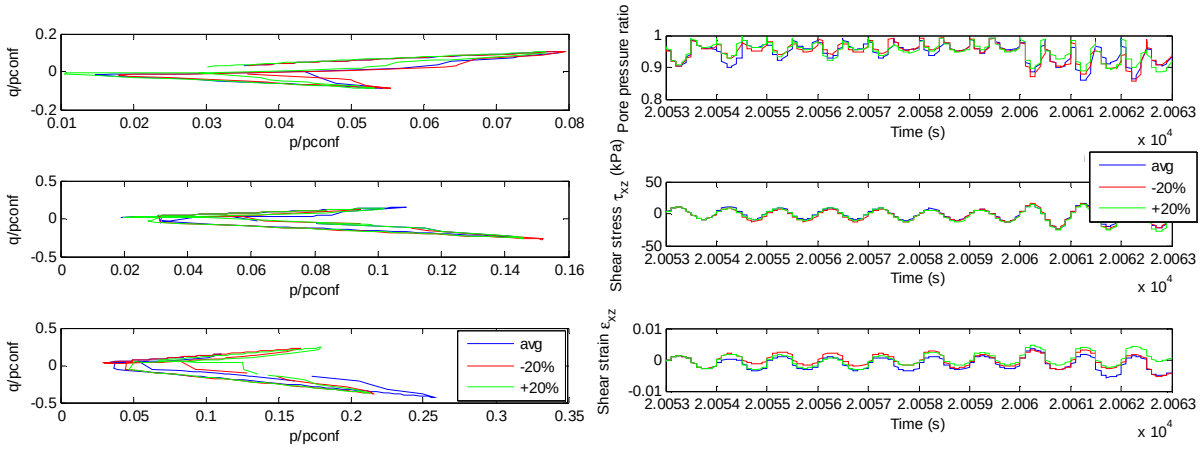

Figure 7. *q/p_{conf} vs p/p_{conf} paths (liquefaction) and pore pressure ratio, shear stress and shear strain time history (after initial liquefaction) considering variation of c_z*

4.3. Fitting the Model to the Laboratory Results

Hence, the value of parameters h_0, c_h and m still had to be determined. This was done by fitting the numerical model to the MDTT results. From the sensitivity analysis, the most relevant of these parameters was c_h and then h_0. Due to its irrelevant influence on the response for the monotonic sensitivity analysis, the used value of m was the reference value in Table 3. Therefore, parameter c_h was fitted first, followed by h_0. Small adjustments in n^b and A_0 were made as well. As a result, the chosen values for the parameters were: $c_h = 1.33$, $h_0 = 6.05$, $n^b = 4.50$ and $A_0 = 1.25$.

5. CONCLUSION

An immersed tunnel case-study, supported on liquefiable alluvial Tagus river sands, was presented, providing context to this work. MDTTs were executed to characterize stress-strain behaviour of Tagus river sand and calibrate the M-D model. CUTTs were also performed, highlighting the dynamic behaviour of the sand.

Some parameters of the M-D model were directly determined from triaxial tests, while others (h_0 and c_h) were determined by fitting the model to the laboratory results, after carrying out an extensive sensitivity analysis. From this sensitivity study, the most significant parameters to consider for monotonic loading were $\boldsymbol{c_h}$, $\boldsymbol{n^b}$and $\boldsymbol{A_0}$ and, in a joint sensitivity analysis, $\boldsymbol{c_h}$ **and** $\boldsymbol{h_0}$, as well as $\boldsymbol{c_h}$ **and** $\boldsymbol{A_0}$. Regarding cyclic loading, before initial liquefaction, the most relevant parameters were $\boldsymbol{G_0}$, $\boldsymbol{m}$, $\boldsymbol{h_0}$ and $\boldsymbol{c_h}$.

Both the calibration framework and the results of the sensitivity analysis presented here can provide designers with an understanding of the model parameters effects' on its performance and guide them in implementing a complex model into their designs.

ACKNOWLEDGEMENT

Luís Miranda was supported by "Fundação para a Ciência e Tecnologia" (FCT), through PhD scholarship SFRH/BD/99581/2014. Available geotechnical information from various surveys, namely borehole logs and SPTs, was kindly provided by Administração do Porto de Lisboa.

REFERENCES

[1] Ingerslev, C., Kyiomya, O., 1997. "*Earthquake Analysis*", Tunnelling and Underground Space Technology, 12(2):157–162.

[2] Serra, J. B., 1998. "*Caracterização experimental e modelação numérica do comportamento cíclico de solos não coesivos. Aplicação à engenharia sísmica*", Ph.D. Thesis, Universidade Técnica de Lisboa, Instituto Superior Técnico, Portugal, 282 pages.

[3] Georgiannou V. N., Tsomokos A., Stavrou K., 2008. "*Monotonic and cyclic behaviour of sand under torsional loading*", Géotechnique, 58(2):113–124.

[4] Manzari M. T., Dafalias Y. F., 1997. "*A critical state two-surface plasticity model for sands*", Géotechnique, 47(2):255–272.

[5] Dafalias, Y. F., Manzari, M. T., 2004. "*Simple Plasticity Sand Model Accounting for Fabric Change Effects*", J Eng Mech, 130(6):622–634.

[6] Cheng, Z., Dafalias, Y. F. and Manzari, M. T., 2013. "*Application of SANISAND Dafalias-Manzari model in FLAC 3D*", Continuum and Distinct Element Numerical Modeling in Geomechanics, Paper 09-03, 22-24 October 2013, Hangzhou, P.R. China.

[7] Papadimitriou, A. G., Bouckovalas, G. D., Dafalias, Y. F., 2001. "*Plasticity model for sand under small and large cyclic strains*", J Geotech Geoenvironmental Eng, 127(11):973–983.

[8] University of Berkeley, California. OpenSees, retrieved from http://OpenSees.berkeley.edu/.

[9] Zienkiewicz, O. C. and Shiomi, T., 1984. "*Dynamic behavior of saturated porous media; the generalized Biot formulation and its numerical solution*", Int J Num Methods Geomech, 8:71-96.

[10] Miranda, L., Barbosa, A., Serra, J., Caldeira, L., 2017. "*Parameter sensitivity analysis of the Manzari-Dafalias model for modelling the cyclic response of a sand*", 16th WCEE, 9-13 January 2017, Santiago, Chile, https://goo.gl/zhngnq.